# Intrinsic aspect of V-shaped switching in ferroelectric liquid crystals: Biaxial anchoring arising from peculiar short axis biasing in the molecular rotation around the long axis

Naoki Hayashi and Tatsuhisa Kato
*Institute for Molecular Science, Myodaiji, Okazaki 444-8585, Japan*

Tomohiro Ando
*Department of Kansei Engineering, Shinshu University, Ueda 386-8567, Japan*

Atsuo Fukuda
*Department of Electronic and Electrical Engineering, Trinity College, University of Dublin, Dublin 2, Ireland*

Sachiko Kawada and Shinya Kondoh
*Citizen Watch Co., Ltd., Tokorozawa 359-8511, Japan*

(Received 26 December 2002; revised manuscript received 11 April 2003; published 11 July 2003)

To clarify the intrinsic aspect of practically usable thresholdless V-shaped switching in ferroelectric liquid crystals, we have observed textures and measured polarized Raman scattering as well as optical transmittance in a thin homogeneous cell of a single compound by applying an electric field. The results indicate that the so-called surface stabilized ferroelectric states are destabilized, and that there exist rather stable two domains with broad and narrow molecular orientational distributions, both of which show the almost ideal V-shaped switching with considerably low transmittance at the tip of the V. We have concluded that the main cause of the V-shaped switching is the biaxial anchoring on the substrates coated with polyimide, which makes the most polarizable short axis normal to the substrates. It is in competition with the ordinary anchoring that favors the director parallel to the substrates, when the material has such a bulk intrinsic property that this short axis is parallel to the tilt plane. The competition makes the total anchoring energy almost independent of the azimuthal angle and gives rise to the V-shaped switching.

DOI: 10.1103/PhysRevE.68.011702 PACS number(s): 61.30.Hn, 61.30.Gd, 77.80.Fm, 77.84.Nh

## I. INTRODUCTION

The thresholdless V-shaped switching, characterized by the field-induced continuous reorientation of a spatially uniform optical axis, was observed in two kinds of mixtures, which consist of compounds with molecular structures basically similar to those of the prototyped antiferroelectric liquid crystals, MHPOBC and TFMHPOBC [1–3]. Because of its potential applications to liquid crystal displays with active matrix electrodes (AM-LCDs) [4,5], many liquid crystal materials (single compounds and mixtures) have been developed under the guiding principle of frustrating ferroelectricity and antiferroelectricity [6–9]. It has been well established that any liquid crystals, ferroelectric, ferrielectric, and antiferroelectric, may show the V-shaped switching; the frustration must be a bulk property essential for its appearance. At the same time, a puzzling statement has been repeatedly made in previous publications; the suitable materials for the V-shaped switching show an apparently single ferrielectric phase in the bulk over a wide ($\sim 100\,^{\circ}\mathrm{C}$) temperature range. In fact, such is the electric-field dependence of conoscopic figures in the V-shaped switching materials that the melatopes emerge parallel to the applied electric field. Concerning this peculiar melatopes appearance, Matsumoto *et al.* recently clarified another essential property in the bulk [10]. They concluded that the ''ferrielectric phase'' is a frustrated ferroelectric (smectic-$C^*$) Sm-$C^*$ phase, where the most easily polarizable molecular short axis is characteristically biased in the rotation around the molecular long axis.

There are two equivalent biased directions in Sm $C^*$ because of the $C_2$ symmetry axis normal to the tilt plane; the averaged short axis, as a whole, or the most easily polarizable macroscopic short axis should be in the tilt plane or vertical to it. Accordingly, Sm $C^*$ in the bulk may be grouped into two, ordinary and frustrated. In ordinary Sm $C^*$, the short axis is vertical and hence the minimum index-of-refraction axis is parallel to the tilt plane; the melatopes appear perpendicularly to the applied electric field. In frustrated Sm $C^*$, on the other hand, the short axis is parallel and hence the minimum index-of-refraction axis is vertical to the tilt plane; the melatopes emerge parallel to the field. Matsumoto *et al.* further assumed, concerning the surface property of polyimide aligning films, such biaxial anchoring that the most easily polarizable macroscopic short axis is liable to become perpendicular to the substrates. In other more intuitive words, the phenyl rings and carbonyl moieties would like to become perpendicular to the polyimide aligning films. In ordinary Sm $C^*$, not only the director anchoring but also this biaxial anchoring of the short axis constructively stabilizes the so-called surface stabilized states. In frustrated Sm $C^*$, on the other hand, these two kinds of anchoring result in a competition so that the total anchoring energy becomes almost independent of the azimuthal angle specifying the position on the Sm-$C^*$ tilt cone. Consequently, the relatively weak anchoring due to rubbing must align in-plane directors; when the chiral twisting power is large, the distribution around the rubbing direction may become broad. In other words, the molecular alignment critically depends on the

 ©2003 The American Physical Society

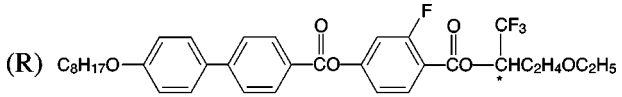


isotropic - 107.7 °C - Sm *A* - 104.7 °C - Sm *C** - 39 °C - crystal

FIG. 1. Chemical structure and phase sequence of the liquid crystal used.

substrate interface conditions and hence a variety of alignments have actually been observed [11–13].

In this way, three basic essentials for the V-shaped switching in the group of developed materials [6,7] are the followng: (1) the frustration between ferroelectricity and antiferroelectricity, (2) the peculiarly biased molecular rotation around the long axis that keeps the most easily polarizable macroscopic short axis in the tilt plane, and (3) the biaxial anchoring favoring this short axis perpendicular to the substrates coated with polyimide aligning films. The purpose of this paper is to advance the understanding of the V-shaped switching in terms of these three essentials. The paper is arranged as follows. After describing the experimental setups and sample cell preparations, Sec. II reviews how to obtain the apparent order parameters, $\langle P_2 \rangle_{\mathrm{app}}$ and $\langle P_4 \rangle_{\mathrm{app}}$, from the polarized Raman intensities, $I_{Z,\mathrm{meas}}(\omega)$ and $I_{X,\mathrm{meas}}(\omega)$. Section III summarizes experimentally obtained results, i.e., textures, electro-optical responses, $\langle P_2 \rangle_{\mathrm{app}}$ and $\langle P_4 \rangle_{\mathrm{app}}$, and in particular, those measured at the tip of the V by time-resolved polarized Raman scattering. In order to understand the V-shaped switching, we try to reconstruct the molecular orientational distribution function at the tip of the V; Sec. IV describes the reconstruction method. In Sec. V, we explain how the biaxial anchoring destabilizes the so-called surface stabilized states; this leads to the V-shaped switching as is being experimentally observed. Section VI gives the conclusion.

## II. EXPERIMENT

The liquid crystal single compound shown in Fig. 1 was sandwiched between two indium-tin-oxide-plated glass substrates, which were coated with ~20-nm-thick polyimide (Nissan, RN-1266) as an aligning reagent. Only one of the two substrates was rubbed in one direction and sense. The gap of the cell was set at 1.6 $\mu$m by spacer particles. The sample cell was mounted in an oven, the temperature of which was adjusted by a controller (Yokogawa, UP550) within an accuracy of $\pm 0.1\,^{\circ}$C. In this paper, all experiments were carried out at 60 °C. The spontaneous polarization of the sample is $\approx 250$ nC cm$^{-2}$ ($2.5\times10^{-3}$ C m$^{-2}$).

Polarized Raman scattering was measured in the backward scattering geometry. The green light at 514.5 nm from an Ar-ion laser (Spectra-Physics, BeamLok 2060) was used for excitation. Figure 2 schematically shows the geometry used in polarized Raman scattering measurements. The laser light is incident along the *Y* axis and its polarization direction is parallel to the *Z* axis. Here, the *X*, *Y*, and *Z* axes constitute the right-handed Cartesian coordinate frame and the *XZ* plane is parallel to the substrates. The incident laser light with a power of 0.5 W is focused onto the sample and the

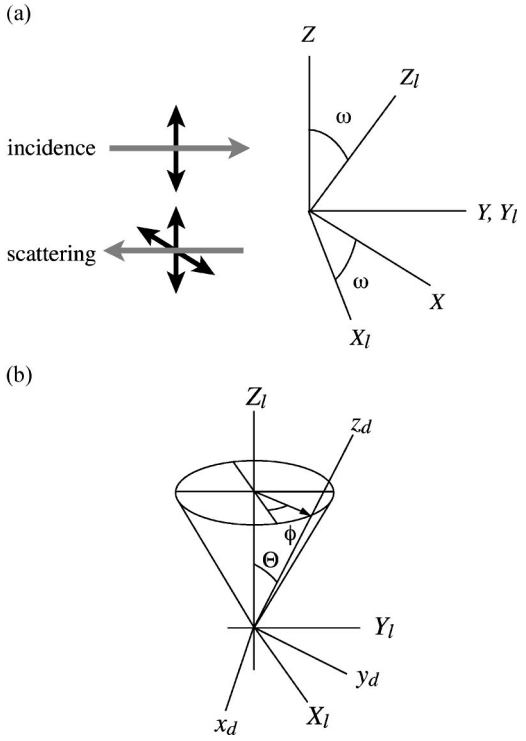


FIG. 2. Coordinate systems in polarized Raman scattering measurements: (a) the laboratory fixed coordinate frame $(X,Y,Z)$ and (b) the smectic layer coordinate frame $(X_l,Y_l,Z_l)$ and the local in-layer director coordinate frame $(x_d,y_d,z_d)$. The *Y* and $Y_l$ axes are taken to coincide with each other, since no chevron structure is considered. Substrates are perpendicular to the *Y* axis and an electric field is applied along it.

beam diameter is $\approx 700$ $\mu$m. The scattered light going back along the *Y* axis is collected by a telescope lens ($f = 130$ mm and $f/d = 1.3$). After passing through a polarizer and a Raman notch filter, the scattered light is focused onto an optical fiber that transmits the light to a monochromator (Spex, 270M) combined with a multichannel detector (Princeton Instruments, IPDA 512). The slit width of the monochromator is 200 $\mu$m. The *Z*- and *X*-polarized Raman spectra were measured by rotating the sample cell from $\omega = 0°$ to $\omega = 180°$ about the *Y* axis. Here, $\omega$ is the rotation angle of the cell and $\omega = 0°$ indicates that the *Z* axis is parallel to the layer normal. The Raman line at 1600 cm$^{-1}$, assigned to the C—C stretching mode of phenyl ring, is suitable for probing the molecular ordering because this line is well separated from the other lines and, moreover, because the major principal axis of the Raman scattering tensor is almost parallel to the molecular long axis. The *Z*- and *X*-polarized Raman lines at 1600 cm$^{-1}$ were fitted with a Lorentzian curve and the integrated intensities, $I_{Z,\mathrm{meas}}$ and $I_{X,\mathrm{meas}}$, were calculated. The depolarization ratio of the Raman line in the isotropic phase, $R_{\mathrm{iso}} = I_{X,\mathrm{meas}}/I_{Z,\mathrm{meas}}$, is 0.373.

The integrated intensities under no electric field and in the field-induced uniform ferroelectric states were obtained for every 10° from $\omega = 0°$ to $\omega = 180°$; the accumulation time was 50 s. To obtain the integrated intensities at the tip of the V, time-resolved Raman scattering measurement was per-

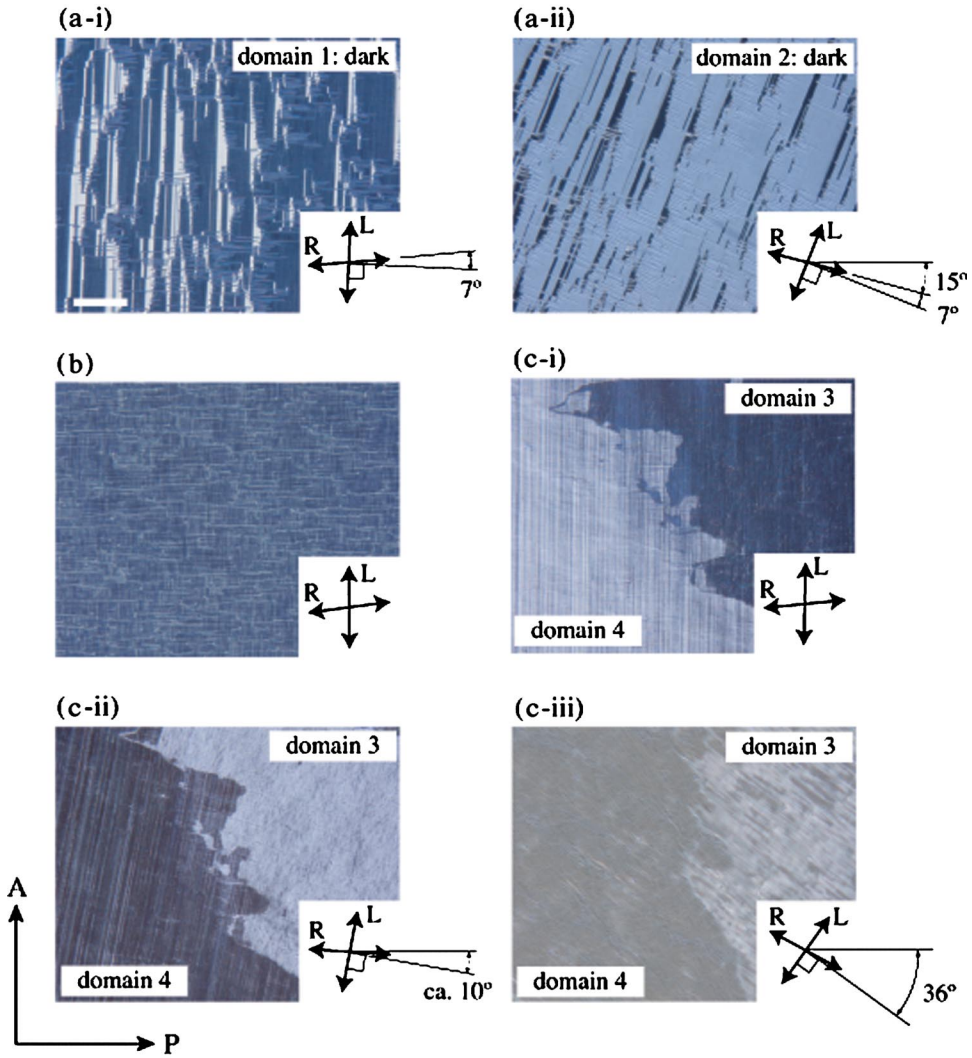


FIG. 3. (Color online) Optical micrographs of textures taken at the virgin state (a-i) and (a-ii), after five cycles of the switching (b), and after the long-term switching (c-i), (c-ii), and (c-iii). The sample cell was placed in such a way that the unrubbed and rubbed substrates comes above and below, respectively. The rotational stage was so adjusted that one of the domains becomes darkest (extinguished). Crossed polarizer axes are parallel and perpendicular to the horizontal edge of each micrograph, which corresponds to the optical axis of extinguished domains. The micrograph (c-iii) was obtained by applying an electric field of 8.6 V $\mu m^{-1}$ and the others were taken without any electric field. The arrow "*L*" indicates the layer direction and the arrow "*R*" indicates the rubbing direction. All images were taken at the same magnification and a white bar drawn bottom left in (a-i) corresponds to 0.1 mm in length.

formed at every 30° by applying a 1-Hz-triangular waveform electric field. The gated pulse with 4 ms width was applied once in a period of 1 Hz to the detector at the tip of the V and the accumulation time was 10 min. The apparent second- and fourth-order orientational order parameters, $\langle P_2 \rangle_{app}$ and $\langle P_4 \rangle_{app}$, were obtained from the integrated intensities as well as the depolarization ratio by using the procedure described in the previous paper [14]. It should be noted that the obtained apparent order parameters include the information not only about the spatial distribution of the local in-plane directors but also about the fluctuations at the molecular level and the imperfect alignment of the smectic layers [14–16].

The intensity of the laser light passing through the cell and a polarizer was detected by a photodiode. The polarization direction of the polarizer is perpendicular to that of the incident laser light. The electro-optic response was monitored for confirming the thresholdless V-shaped switching during the time-resolved polarized Raman scattering measurements. Texture observation by a polarizing optical microscope (Olympus, BX50) was made for testing the quality of alignment in the virgin state, after short-term ($\sim$5 cycles of 1-Hz triangular wave) and long-term (10 hs) switching operations, and before and after the polarized Raman scattering measurements.

## III. RESULTS

Figure 3 summarizes micrographs of a cell taken by a polarizing microscope. The rotational stage was so adjusted that one of the domains becomes darkest. Two domains, "1" and "2," are observed in the virgin state before applying any electric field, the textures of which are shown in Figs. 3(a-i)

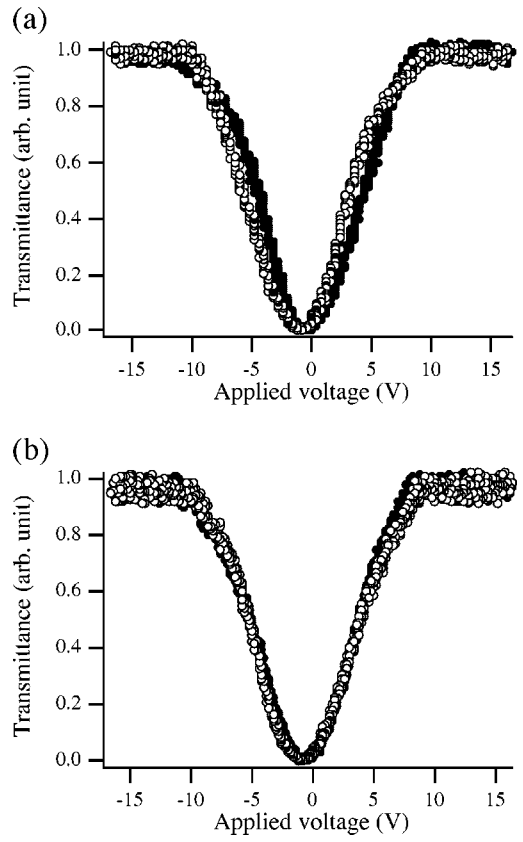


FIG. 4. Electro-optic responses observed in domains 3 (a) and 4 (b). Solid and open circles were obtained by increasing and decreasing the applied electric field, respectively.

and 3(a-ii). In both domains, the interface induced electroclinic effect in the Sm-*A* phase makes the layer normal inclined by $+7°$ (clockwise) from the rubbing direction [17–19]. Domain 1 occupies larger area in the sample cell. Its somewhat bluish, though considerably dark, texture in Fig. 3(a-i) indicates that domain 1 is in the twisted state with a small twisting angle [12,20]. The average optical axis is almost parallel to the layer normal in domain 1. The very uniform dark texture in Fig. 3(a-ii), on the other hand, appears to indicate that domain 2 is in a surface stabilized state [13]. The optical axis makes an angle of $-15°$ (counterclockwise) with the rubbing direction.

By applying five cycles of a triangular waveform electric field (1 Hz, $\pm 10\ \mathrm{V}\,\mu\mathrm{m}^{-1}$), we obtained a texture characterized by many stripes nearly along the layers as given in Fig. 3(b). The texture indicates the same small twisted state as domain 1 except for the stripes. The average optical axis is parallel to the layer normal, although the optical axis of each stripe domain shows some orientational distribution around the averaged one. Since domain 2 disappears, the small twisted state must be more stable than the surface stabilized state.

After switching for ca. 10 h, two newly emerging domains, ''3'' and ''4,'' prevail as shown in Figs. 3(c-i) and 3(c-ii); domain 3 is extinguished and domain 4 is bright in Fig. 3(c-i), while the opposite is true in Fig. 3(c-ii). The texture of the domain 3 closely resembles the one observed in Fig. 3(b), indicating that domain 3 also is in the small twisted state. Domain 4 has the average optical axis tilted by ca. $-10°$ from the layer normal and is characterized by thin stripes parallel to the layer. Further switching results in the

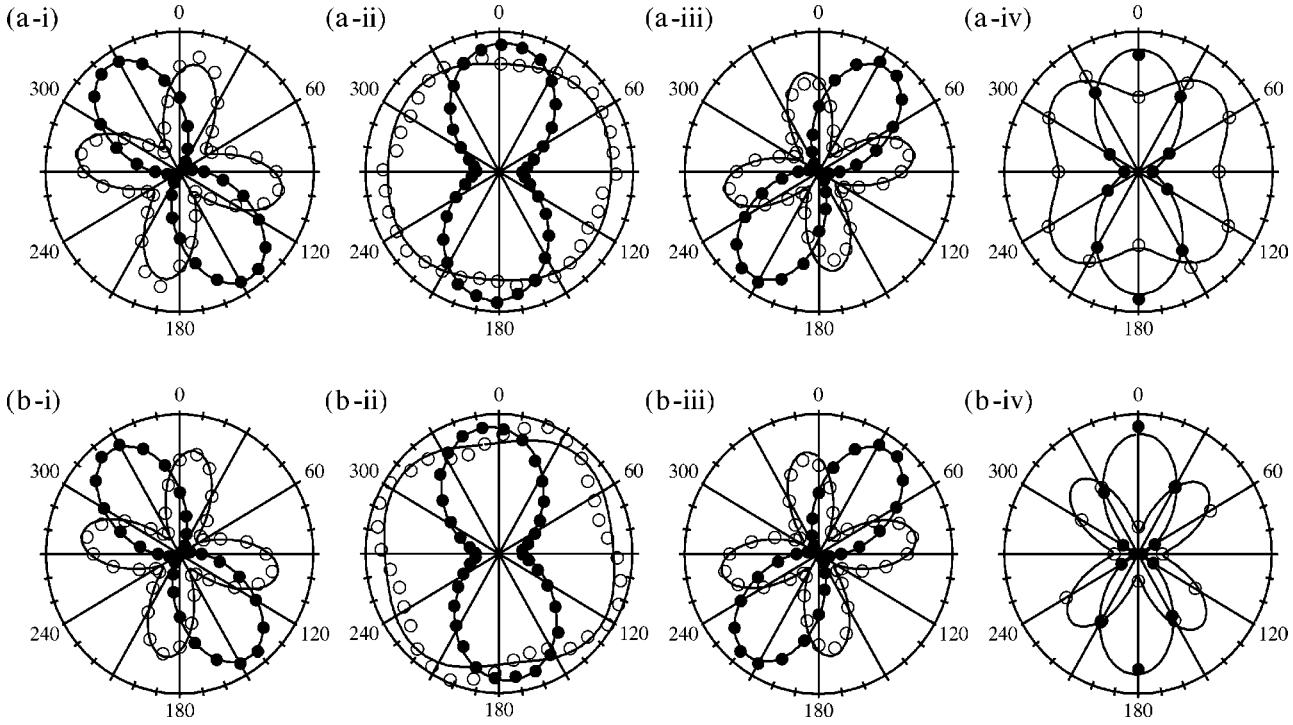


FIG. 5. Polar plots of polarized Raman intensities (in arbitrary units) vs cell rotation angles (in degrees) obtained in domain 3 (a) and domain 4 (b). (i) $8.6\ \mathrm{V}\,\mu\mathrm{m}^{-1}$ (dc), (ii) 0 V (dc), (iii) $-8.6\ \mathrm{V}\,\mu\mathrm{m}^{-1}$, and (iv) at the tip of the V (1 Hz). Solid and open circles show $I_{Z,\mathrm{meas}}(\omega)$ and $I_{X,\mathrm{meas}}(\omega)$, respectively, and $I_{X,\mathrm{meas}}(\omega)$ is enlarged three times.

TABLE I. Orientational order parameters obtained by polarized Raman scattering measurements.

| | Domain 3 | | Domain 4 | |
|---|---|---|---|---|
| $E$ ($\mathrm{V}\,\mu\mathrm{m}^{-1}$) | $\langle P_2\rangle_{\mathrm{app}}$ | $\langle P_4\rangle_{\mathrm{app}}$ | $\langle P_2\rangle_{\mathrm{app}}$ | $\langle P_4\rangle_{\mathrm{app}}$ |
| 0 (dc) | 0.40 | −0.13 | 0.39 | −0.14 |
| 8.6 (dc) | 0.77 | 0.46 | 0.84 | 0.62 |
| −8.6 (dc) | 0.86 | 0.63 | 0.84 | 0.64 |
| the tip of V (1 Hz) | 0.49 | 0.00 | 0.76 | 0.52 |

expansion of domain 4 at the expense of domain 3. Figure 3(c-iii) shows the texture obtained by applying an electric field of 8.6 $\mathrm{V}\,\mu\mathrm{m}^{-1}$, which is high enough to attain a field-induced uniform state. Many lines emerge along the layer normal in domain 3, while few are observed in domain 4, although these lines are not clearly reproduced in Fig. 3(c-iii). These lines must indicate the horizontal chevron structure which are frequently observed in the field-induced uniform state [21,22], suggesting a difference in the layer structure between domains 3 and 4.

Figures 4(a) and 4(b) illustrate the V-shaped switchings observed in domains 3 and 4, respectively, by applying an electric field of triangular waveform (1 Hz, $\pm 10\ \mathrm{V}\,\mu\mathrm{m}^{-1}$). The electro-optic response in domain 3 exhibits small hysteresis on the way between the tip of the V and the field-induced uniform state, although the tip in the increasing and decreasing processes are located at almost the same position; the critical electric field where the transmittance reaches to the plateau is slightly smaller than the one where the transmittance leaves the plateau. Such a hysteresis is not observed in domain 4. For both domains, the transmittance at the tip of the V is extremely low although the position of the tip is slightly shifted toward the negative electric field. This shift is frequently observed in one-side rubbing cells [11,23]. The saturation voltage $V_{\mathrm{sat}}$ is $\approx 10$ V. Clark *et al.* showed that $V_{\mathrm{sat}}$ is given by $V_{\mathrm{sat}}=2P_0t/\epsilon_{\mathrm{IL}}$ [24], where $t$ is the thickness and $\epsilon_{\mathrm{IL}}$ is the dielectric constant of the alignment layer. Since $P_0=2.5\times10^{-3}\ \mathrm{C\,m}^{-2}$, $t=20$ nm, and $\epsilon_{\mathrm{IL}}=3\epsilon_0$ ($\epsilon_0$ is the vacuum dielectric constant), $V_{\mathrm{sat}}=4$ V is predicted which is only one half of the experimental value.

Figures 5(a) and 5(b) show the results of polarized Raman scattering measurements in domains 3 and 4, respectively. The Raman intensities, $I_Z(\omega)$ and $I_X(\omega)$, are plotted as a function of the cell rotation angle $\omega$. Here, $\omega=0$ indicates that the layer normal is parallel to the polarization direction of incident laser light. The polarized Raman intensities from 190° to 350° are duplicates of the observed intensities from 10° to 170°. The maximum direction of $I_{Z,\mathrm{meas}}$ corresponds to the averaged molecular orientation. Figures 5(a-ii) and 5(b-ii) show the results obtained under no electric field. Figures 5(a-i), 5(a-iii), 5(b-i), and 5(b-iii) are the results in the field-induced uniform states obtained by applying dc electric fields. Figures 5(a-iv) and 5(b-iv) were measured by the time-resolved technique at the tip of the V during the switchings shown in Figs. 4(a) and 4(b), respectively. The maximum point of $I_{Z,\mathrm{meas}}(\omega)$ in Fig. 5(a-ii) is ca. 2° whereas that in Fig. 5(b-ii) is ca. −10°; these are consistent with the results observed by a polarizing optical microscope and is given in Fig. 3(c-i) and 3(c-ii). In the field-induced uniform states shown in Figs. 5(a-i), 5(a-iii), 5(b-i), and 5(b-iii), the maximum points of $I_{Z,\mathrm{meas}}(\omega)$ are tilted by the averaged molecular tilting angle from the layer normal. At the tip of the V, the averaged molecular orientations are parallel to the layer normal in both domains as seen in Figs. 5(a-iv) and 5(b-iv). However, a significant difference is noticed in the profile of $I_{X,\mathrm{meas}}(\omega)$. The rather round profile of $I_{X,\mathrm{meas}}(\omega)$ in Fig. 5(a-iv) suggests a broad molecular orientational distribution, while the distinct four-leaf clover profile in Fig. 5(b-iv) indicates a narrow distribution.

TABLE II. Orientational order parameters calculated by using Eqs. (1) and (2). The molecular tilt angle used was $\Theta=35.1°$, which was determined experimentally by applying a dc electric field of 8.6 $\mathrm{V}\,\mu\mathrm{m}^{-1}$.

| | | Domain 3 | | Domain 4 | |
|---|---|---|---|---|---|
| | $\sigma_{\mathrm{d}}$ (degree) | $\langle P_2\rangle_{\mathrm{app}}$ | $\langle P_4\rangle_{\mathrm{app}}$ | $\langle P_2\rangle_{\mathrm{app}}$ | $\langle P_4\rangle_{\mathrm{app}}$ |
| Equation (1) | 0 | 0.74 | 0.42 | 0.76 | 0.49 |
| | 20 | 0.65 | 0.25 | 0.66 | 0.28 |
| | 40 | 0.50 | 0.03 | 0.50 | 0.02 |
| | 60 | 0.43 | −0.06 | 0.43 | −0.09 |
| Equation (2) | | 0.41 | −0.09 | 0.41 | −0.13 |

The fitting procedure described in the previous paper [14] provides apparent orientational order parameters, $\langle P_2\rangle_{\mathrm{app}}$ and $\langle P_4\rangle_{\mathrm{app}}$, together with the apparent molecular tilt angle from the layer normal, $\Theta_{\mathrm{app}}$. Table I lists $\langle P_2\rangle_{\mathrm{app}}$ and $\langle P_4\rangle_{\mathrm{app}}$, and $\Theta_{\mathrm{app}}$'s are 35.1° and 36.0° in domains 3 and 4, respectively. The difference in $\Theta_{\mathrm{app}}$ between the domains may owe to the horizontal chevron layer structure in domain 3. For the relaxed states without any electric filed, $E=0$ (dc), the orientational order parameters for both domains are very small. The surface stabilized states are not yet attained. These may be caused by a residue of helical structure and/or many stripes observed in Figs. 3(c-i) and 3(c-ii). It should be noticed that the order parameters at $E=8.6\ \mathrm{V}\,\mu\mathrm{m}^{-1}$ in domain 3 are lower than the other three uniform field-induced uniform states. This suggests that the molecular orientational distribution in the cell at $E=8.6\ \mathrm{V}\,\mu\mathrm{m}^{-1}$ is much different from the others. At the tip of the V, the order parameters obtained in domain 3 are very small while those in domain 4 are rather large.

## IV. MODEL CALCULATION

In order to clarify the process or mechanism of the V-shaped switching, it is useful to presuppose some orientational distribution functions of local in-layer directors that can reproduce the apparent order parameters experimentally obtained at the tip of the V. The geometry used in this model calculation is illustrated in Fig. 2(b). The director tilt angle $\Theta$ is considered as constant throughout the sample at a particular temperature, because any change in $\Theta$ critically varies the smectic layer thickness and hence results in a remarkable

free energy increase. Hence, any rather narrow distributions in the azimuthal angle $\phi$ can be simply written as

$$f_d(\phi,\theta,\chi)=\frac{1}{4\pi\sqrt{2\pi}\sigma_{\rm d}}\exp\left[-\frac{(\phi-\pi/2)^2}{2\sigma_{\rm d}^2}\right]\delta(\theta-\Theta), \tag{1}$$

while extremely broad distributions in $\phi$ are approximated by the uniform distribution

$$f_d(\phi,\theta,\chi)=\delta(\theta-\Theta)/(8\pi^2). \tag{2}$$

Here, $\phi$, $\theta$, and $\chi$ are the Euler angles of the local in-layer director coordinate frame ($x_d$, $y_d$, and $z_d$) in the smectic layer coordinate frame ($x_l$, $y_l$, and $z_l$), $\delta$ is the dirac delta function, and $\sigma_d$ in Eq. (1) refers to the standard deviation. The distribution with $\sigma_d=0°$ can also be written as $\delta(\phi-\pi/2)$; with increasing $\sigma_d$, the distribution becomes broader. Note that, as seen in Figs. 5(a-iv) and 5(b-iv), the averaged molecular orientations at the tip of the V are almost parallel to the normal both in domains 3 and 4, i.e., $\phi=\pi/2$. It has already been explained in detail in the previous papers [14,15] how to obtain $\langle P_2\rangle_{\rm app}$ and $\langle P_4\rangle_{\rm app}$ from these distribution functions together with some experimentally obtained data.

Table II lists the results of such model calculations in domains 3 and 4. A small difference between the results calculated in domains 3 and 4 results from the fact that the order parameters of the field-induced uniform states are different between domains 3 and 4. However, the difference is so small that it makes no significant meaning in the following discussion. The apparent order parameters, $\langle P_2\rangle_{\rm app}$ and $\langle P_4\rangle_{\rm app}$, calculated by Eq. (1) with $\sigma_d=40°$ and $0°$ almost reproduce the experimentally obtained ones at the tip of the V in domains 3 and 4, respectively. One may consider that the broad distribution in domain 3 is due to the polarization-stabilized twisted structure proposed by Rudquist *et al.* [25]. The proposed structure has a thick bulk slab with the uniform orientation of molecules, which is stabilized by the stiffening effect of the high spontaneous polarization, and very thin slabs with twisted structure near two substrate surfaces. The spatial distribution about the azimuthal angle of the in-layer director along the $Y_l$ axis is characterized by the coherence length $\xi$, which is given by

$$\xi=\sqrt{\frac{K\epsilon}{P_0^2}}. \tag{3}$$

Here, $K$ is the elastic constant, $\epsilon$ is the dielectric constant, and $P_0$ is the spontaneous polarization of the sample. When $P_0=2.5\times10^{-3}$ C m$^{-2}$, $K\sim10^{-11}$ N, and $\epsilon=10\epsilon_0=8.9\times10^{-11}$ F m$^{-1}$ for typical values, $\xi=\sim10$ nm is obtained. This condition gives $\langle P_2\rangle_{\rm app}=0.70$ and $\langle P_4\rangle_{\rm app}=0.40$, whereas the experimental values are 0.49 and 0.00, respectively. Hence, the broad distribution in the domain 3 cannot be explained by the assumed polarization-stabilized twisted structure [25].

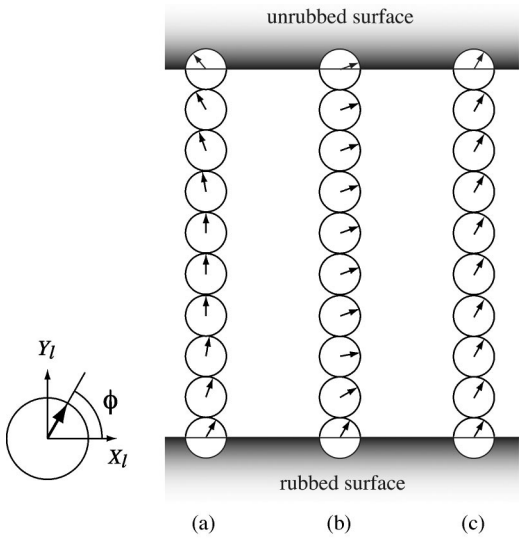


FIG. 6. Possible orientational structures of in-layer directors along the cell thickness; the small twist structure (a), the surface stabilized structure (b), and the uniform structure (c). The arrows in the circles indicate the azimuthal direction of the local in-plane directors with respect to the $X_l$ axis. The angle between the arrow and the alignment layer surface is $\phi$. No chevron layer structure is considered.

## V. DISCUSSION

We admit that our cell fabrication method was inappropriate at least in the following two respects: (1) we rubbed only one substrate because of a difficulty in preparing cross rubbing in order to compensate a rather large interface-induced electroclinic effect [17–19] and (2) we had to use RN-1266 with slightly low performance because a much better aligning agent RN-1299 absorbs the 514.5-nm laser light [12]. The inappropriateness surely caused the temporal variation of textures and molecular orientational distributions after the switching operations. However, as explained in the following, it very much helped us to understand the important role played by the biaxial anchoring [10] as well as the frustration between ferroelectricity and antiferroelectricity [6–9]. The compound here investigated was reported as a ferrielectric liquid crystal [6]. As explained in the Introduction, however, it is much more natural to consider that the ''ferrielectric'' phase is a ferroelectric Sm-$C^*$ phase in which the melatopes in the helix-unwound state may emerge parallel to the applied electric field contrary to those in ordinary Sm $C^*$ observed in DOBAMBC, MHPOBC, etc. There is no inevitability for the emergence of the perpendicular melatopes in Sm $C^*$ [10], because whether the minimum index-of-refraction axis is parallel or perpendicular to the tilt plane critically depends on the biasing direction of the most polarizable short axis in the molecular rotation around the long axis. Note that the melatopes appear in a plane containing the viewing direction and the minimum index-of-refraction axis. In fact, the surface stabilized state observed as domain 2 in Figs. 1(a-i) and 1(a-ii) supports the identification of Sm $C^*$; the apparently small tilt angle shown in Fig. 3(a-ii) as compared with that in Fig. 3(c-iii) must result from the chevron

structure together with the pretilt on the substrates as will be explained in connection with Fig. 6(b). Since domain 2 is not stable, there must exist some mechanism that destabilizes the surface stabilized states.

Let us consider how the *biaxial* anchoring causes the destabilization and this results in the V-shaped switching. Domains 3 and 4 that exist rather stably in a sample cell have the different azimuthal angle distributions of the in-layer directors at the tip of the V, but still show the very similar thresholdless V-shaped electro-optical responses. The distribution is broad in domain 3, while it is very narrow in domain 4. This fact indicates that the ''charge stabilization'' and/or the ''polarization stiffening'' [24,25], if any, does not play a decisive role. The broad distribution may partially be due to the very short helical pitch ($\sim$170 nm) [6]; however, the helical unwinding process is not dominant in the V-shaped switching as clearly seen in the very narrow distribution in domain 4. Some randomization process that makes the distribution broad must be necessary for explaining both the very low orientational order parameters at the tip of the V and the apparently uniform switching. Moreover, since the distributions in the relaxed states at $E=0$ V $\mu$m$^{-1}$ (dc) are different from those at the tip of the V both in domains 3 and 4, it is clear that the interaction between the liquid crystal and the alignment layer molecules affects the molecular orientational distributions during the switching processes. The interaction is usually described by the anchoring energy for directors on the substrates, $f_A$.

Taking the smectic layer frame $(X_l, Y_l, Z_l)$ as shown in Fig. 6, we write $f_A$ as the sum of two contributions from the upper unrubbed and the lower rubbed substrates,

$$f_A = f_{A,l} + f_{A,u}, \tag{4}$$

where

$$f_{A,l} = \text{const} - A_{n,l}\cos^2\phi(0) - A_{b,l}\cos^2\phi(0) - A_{p,l}\cos\phi(0) - A_{i,l}\sin\phi(0) \tag{5}$$

and

$$f_{A,u} = \text{const} - A_{n,u}\cos^2\phi(L) - A_{b,u}\cos^2\phi(L) + A_{p,u}\cos\phi(L). \tag{6}$$

Here, $\phi(0)$ and $\phi(L)$ are the azimuthal angles specifying the directors on the lower rubbed and the upper unrubbed substrates. The second and fourth terms represent the ordinary nonpolar and polar anchoring energies [26]. The fourth polar terms are considered not so large on the polyimide aligning films. The last term in Eq. (5) is the in-plane anchoring energy due to rubbing introduced by Panarin *et al.* [27]. Increasing the rubbing strength leads to a larger value of $A_{i,l}$ [17,27]. No corresponding term exists in Eq. (6) because the upper substrate was not rubbed. All the coefficients of these terms are usually considered to be always positive. The biaxial anchoring is given by the third terms in both Eqs. (5) and (6). As explained in the Introduction, Matsumoto *et al.* [10] assumed that the most easily polarizable macroscopic short axis is liable to become perpendicular to the substrates. It results in a competition with the ordinary anchoring of directors being parallel to the substrates, when the material has such a bulk intrinsic property that the most easily polarizable macroscopic short axis is parallel to the tilt plane. The coefficients can be written as

$$A_{b,l} = A_{b,u} = a_b \cos(2\psi_p), \tag{7}$$

where $\psi_p$ is the angle between the most easily polarizable molecular short axis and the Sm-$C^*$ tilt plane normal [10]. Since the conoscopic observation indicates that $\pi/4 < \psi_p < 3\pi/4$ in the compound here investigated, the second and third terms partly cancel out with each other due to a change in the signs of $A_{b,l}$ and $A_{b,u}$ based on the angle $\psi_p$.

The $\phi$ dependence of the polar and nonpolar interaction terms must become considerably reduced. Consequently, on the *rubbed* surface, the in-plane anchoring term dominantly determines the molecular orientation, making $\phi \sim \pi/2$ stable as already confirmed by some other experimental results [12,13,20]. The interface-induced electroclinic effect [17–19] and the weak polar interaction term with a positive $A_{p,l}$ gives a slight deviation from $\phi=\pi/2$ toward $\phi=0$. Meanwhile, on the *unrubbed* surface, the $\phi$ dependence of $f_{A,u}$ is also small; since there is no in-plane anchoring, $f_{A,u}$ must have two minima at $\phi\sim 0$ and $\phi\sim\pi$ for $-A_{n,u}-A_{b,u}<0$, but has only one minimum at $\phi\sim\pi/2$ for $-A_{n,u}-A_{b,u}>0$. When the two minima exist, either of $\phi\sim 0$ or $\phi\sim\pi$ is more stable than the other depending on the sign of $A_{p,u}$. In the virgin state of the sample, the small twisted structure of domain 1 and the surface stabilized structure of domain 2 are observed. Hence, we conclude that $-A_{n,u}-A_{b,u}<0$. By taking into account of the small $\phi$ dependence of $f_A$, the elastic energy, and the stiffening effect, two structures illustrated in Figs. 6(a) and 6(b) are probable. When the phase transition from Sm $A$ to Sm $C^*$ occurs epitaxially from the unrubbed surface, $\phi\sim 0$ and $\phi\sim\pi$ are equally possible. If the phase transition starts with $\phi\sim 0$, the small twist structure is formed as shown in Fig. 6(a). Because of the elastic force and the stiffening effect, the molecular orientation along the cell thickness or the $Y_l$ axis tends to be uniform in the bulk and $\phi$ on the unrubbed surface approaches to $\pi/2$ from $\pi$ because of the small $\phi$ dependence of $f_A$ [24,28,29]. Meanwhile, if the phase transition starts with $\phi\sim\pi$, the surface stabilized structure is formed as shown in Fig. 6(b). Relatively thin alignment layers ($\sim$20 nm) can maintain the surface stabilized state [30]. Since domain 2 changed into domain 1 after a few cycles of the switching operation, the surface stabilized structure is a metastable state. The metastability of the surface stabilized structure may result from the unfavorable sign of $A_p$, the stiffening effect, and the elastic force in the bulk because $\phi\sim\pi/2$ is always stable on the rubbed surface. In the similar way, if the phase transition takes place from the rubbed surface, only the small twist structure is stabilized.

Now we try to understand the switching process in domains 3 and 4 together with the evolution from domain 3 to domain 4. In the early stage of the switching operation, the interaction between the liquid crystal and the alignment layer molecules is relatively strong and the motions of the liquid crystal molecules are disturbed by the irregularity of the

alignment layer surface. The synclinic molecular arrangement between adjacent layers is easily broken and cannot be recovered immediately because of the reduced interlayer molecular correlation by the frustration between the ferroelectricity and antiferroelectricity. Therefore, the randomization process is introduced and the distribution of the local in-layer directors must be broadened at the tip of the V as observed in domain 3. The relatively strong interaction causes some hysteresis of the electro-optic response shown in Fig. 4(a). It must also be responsible for the emergence of the horizontal chevron structure in domain 3. In domain 4, the long-term switching operation and the laser light irradiation produces a large number of free ions due to the decomposition of the alignment layer [12]. The increased free ions reduce the interaction between the liquid crystal and the alignment layer molecules, namely, both the polar and nonpolar interaction in Eqs. (5) and (6). The $\phi$ dependence of $f_A$ is almost lost on the unrubbed surface, although the favored orientation is still parallel to the rubbing direction on the rubbed surface due to the in-plane anchoring. Consequently, the molecular orientation becomes uniform and parallel to the rubbing direction [12]. The reduced interaction hardly disturbs the uniform molecular alignment, as shown in Fig. 6(c), even in the whole switching process. The texture under a high electric field as seen in Fig. 3(c-iii) and the V-shaped switching with no hysteresis observed in Fig. 4(b) support this inference. The absence of the horizontal chevron structure may also indicate the reduced anchoring in both the polar and nonpolar interactions in Eqs. (5) and (6).

## VI. CONCLUSION

We have observed textures and measured polarized Raman scattering as well as optical transmittance in a thin homogeneous cell of a single compound by applying an electric field. It becomes clear that the so-called surface stabilized ferroelectric states are actually destabilized and that there exist rather stable two domains with broad and narrow molecular orientational distributions, both of which show the almost similar, rather ideal thresholdless V-shaped switching. The molecular distributions at the tip of the V is not essential; hence, charge stabilization or polarization stiffening [24,25] does not play any decisive role. What is essential is the biaxial anchoring on the substrates coated with polyimide [10], which makes the most polarizable short axis normal to the substrates. It results in a competition with the anchoring of the director parallel to the substrates, when the material has such a bulk intrinsic property that the short axis is parallel to the tilt plane. Consequently, the phenomenon of the practically usable thresholdless V-shaped switching is not apparent, contrary to the view expressed by Blinov *et al.* [31], and depends on the intrinsic properties of the materials as well as the cell interface characteristics [6,7,10]. Moreover, another intrinsic property, the frustration between ferroelectricity and antiferroelectricity [6–10], assures the extremely reduced interlayer tilting correlation and hence the field-induced continuous reorientation of a spatially uniform optical axis without forming any visible domains.

## ACKNOWLEDGMENTS

We would like to thank Mitsubishi Gas Chemical Company, Inc. and Nissan Chemical Industries, Ltd. for supplying the materials. One of the authors (A.F.) acknowledge Science Foundation Ireland.

[1] A. Fukuda, in *Proceedings of the 15th International Display Research Conference (Asia Display '95), Hamamatsu, Japan*, (Society for Information Display, San Jose, CA, 1995), p. 61.

[2] S. Inui, N. Iimura, T. Suzuki, H. Iwane, K. Miyachi, Y. Takanishi, and A. Fukuda, J. Mater. Chem. **6**, 671 (1996).

[3] C. Tanaka, T. Fujiyama, T. Maruyama, and S. Nishiyama, in *Abstracts of 1995 Japanese Liquid Crystal Conference, Sendai, Japan* (Japanese Liquid Crystal Society, Tokyo, 1995), p. 250.

[4] H. Okumura, M. Akiyama, K. Takatoh, and Y. Uematsu, in *Proceedings ('98 Digest) of Society for Information Display International Symposium, Anaheim* (Society for Information Display, San Jose, CA, 1998), Vol. 29, p. 1171.

[5] T. Yoshida, J. Ogura, M. Takei, N. Yazawa, R. Mizusako, S. Ando, H. Wakai, and H. Aoki, in *Proceedings of the 7th International Display Workshops (IDW '00), Kobe, Japan* (Society for Information Display, San Jose, CA, 2000), p. 37.

[6] T. Matsumoto, A. Fukuda, M. Johno, Y. Motoyama, T. Yui, S.S. Seomun, and M. Yamashita, J. Mater. Chem. **9**, 2051 (1999).

[7] M. Takeuchi, K. Chao, T. Ando, T. Matsumoto, A. Fukuda, and M. Yamashita, Ferroelectrics **246**, 1 (2000).

[8] E. Gorecka, D. Pociecha, M. Glogarova, and J. Mieczkowski, Phys. Rev. Lett. **81**, 2946 (1998).

[9] D. Pociecha, M. Glogarova, E. Gorecka, and J. Mieczkowski, Phys. Rev. E **61**, 6674 (2000).

[10] T. Matsumoto, Y. Suzuki, M. Johno, T. Okugawa, M. Takeuchi, and A. Fukuda, Jpn. J. Appl. Phys. **40**, L817 (2001).

[11] A.D.L. Chandani, Y. Cui, S.S. Seomun, Y. Takanishi, K. Ishikawa, H. Takezoe, and A. Fukuda, Liq. Cryst. **26**, 167 (1999).

[12] S.S. Seomun, J.K. Vij, N. Hayashi, T. Kato, and A. Fukuda, Appl. Phys. Lett. **79**, 940 (2001).

[13] S.S. Seomun, V.P. Panov, J.K. Vij, A. Fukuda, and J.M. Oton, Phys. Rev. E **64**, 040701(R) (2001).

[14] N. Hayashi, T. Kato, T. Aoki, T. Ando, A. Fukuda, and S.S. Seomun, Phys. Rev. E **65**, 041714 (2002).

[15] N. Hayashi, T. Kato, T. Aoki, T. Ando, A. Fukuda, and S.S. Seomun, Phys. Rev. Lett. **87**, 015701 (2001).

[16] N. Hayashi, T. Kato, T. Ando, and A. Fukuda, Jpn. J. Appl. Phys. **41**, 5292 (2002).

[17] W. Chen, Y. Ouchi, T. Moses, Y.R. Shen, and K. Yang, Phys. Rev. Lett. **68**, 1547 (1992).

[18] K. Nakagawa, T. Shinomiya, M. Koden, K. Tsubota, T. Kuratate, Y. Ishii, F. Funada, M. Matsuura, and K. Awane, Ferroelectrics **85**, 39 (1988).
[19] J.S. Patel, S.-D. Lee, and J.W. Goodby, Phys. Rev. Lett. **66**, 1890 (1991).
[20] S.S. Seomun, T. Fukuda, A. Fukuda, J.G. Yoo, Y.P. Panarin, and J.K. Vij, J. Mater. Chem. **10**, 2791 (2000).
[21] Y. Takahashi, A. Iida, Y. Takanishi, T. Ogasawara, K. Ishibashi, and H. Takezoe, Jpn. J. Appl. Phys. **40**, 3294 (2001).
[22] R.F. Shao, P.C. Willis, and N.A. Clark, Ferroelectrics **121**, 127 (1991).
[23] S.S. Seomun, T. Gouda, Y. Takanishi, K. Ishikawa, H. Takezoe, and A. Fukuda, Liq. Cryst. **26**, 151 (1999).
[24] N.A. Clark, D. Coleman, and J.E. Maclennan, Liq. Cryst. **27**, 985 (2000).
[25] P. Rudquist *et al.*, J. Mater. Chem. **9**, 1257 (1999).
[26] M.A. Handschy, N.A. Clark, and S.T. Lagerwall, Phys. Rev. Lett. **51**, 471 (1983).
[27] Y.P. Panarin, S.T. MacLughadha, and J.K. Vij, Phys. Rev. E **52**, R17 (1995).
[28] M. Nakagawa and T. Akahane, J. Phys. Soc. Jpn. **55**, 1516 (1986).
[29] M. Copic, J.E. Maclennan, and N.A. Clark, Phys. Rev. E **65**, 021708 (2002).
[30] K.H. Yang, T.C. Chieu, and S. Osofsky, Appl. Phys. Lett. **55**, 125 (1989).
[31] L.M. Blinov, E.P. Pozhidaev, F.V. Podgornov, S.A. Pikin, S.P. Palto, A. Sinha, A. Yasuda, S. Hashimoto, and W. Haase, Phys. Rev. E **66**, 021701 (2002).